Effective Engineering Constants for Micropolar Composites with Imperfect Contact Conditions

Reinaldo Rodríguez-Ramos, V. Yanes, Y. Espinosa-Almeyda, C.F. Sánchez-Valdés, J. Otero, Frédéric Lebon, Raffaella Rizzoni, Michele Serpilli, Serge Dumont, F. Sabina

Effective Engineering Constants for Micropolar Composites with Imperfect Contact Conditions

R. Rodríguez-Ramos, V. Yanes, Y. Espinosa-Almeyda, C. F. Sánchez-Valdés, J. A. Otero, F. Lebon, R. Rizzoni, M. Serpilli, S. Dumont, and F. J. Sabina

Abstract In this work, the homogenization theory is applied within the framework of three-dimensional linear micropolar media. The fundamental results derived by the asymptotic homogenization method to compute the effective engineering moduli for a laminated micropolar elastic composite with centro-symmetric constituents are summarized, in which the interface between the layer phases is considered imperfect spring type. The layers are considered with isotropic symmetry. Non-uniform and, as a particular case, uniform imperfections are assumed, where different imperfection parameters and cell lengths in the y_3-direction are assigned for the analysis. The analytical expressions of the engineering constants related to the stiffness and torque are given as functions of the imperfection parameters. The behavior of the engineering coefficients depending on the imperfection is studied. The influence of the imperfection and the cell length in the direction of the imperfection is observed. The present study allows validating other models and experimental results, as well as the investigation of fracture prediction in laminated composite materials.

R. Rodríguez-Ramos (✉)
Facultad de Matemática y Computación, Universidad de La Habana, San Lázaro y L, Vedado, La Habana, CP 10400, Cuba

PPG-MCCT, Universidade Federal Fluminense, Av. dos Trabalhadores 420, Vila Sta. Cecília, CP 27255-125 Volta Redonda, RJ, Brazil
e-mail: reinaldo@matcom.uh.cu; reinaldorr@id.uff.br

V. Yanes
Escuela Técnica Superior de Ingeniería Aeronáutica y del Espacio, Universidad Politécnica de Madrid, Pza. Cardenal Cisneros 3,, Madrid 28040 Madrid, Spain
e-mail: vh.yanes@upm.es

Y. Espinosa-Almeyda · C. F. Sánchez-Valdés
Instituto de Ingeniería y Tecnología, Universidad Autónoma de Ciudad Juárez, Av. Del Charro 450 Norte Cd. Juárez, Chihuahua, CP 32310, Mexico
e-mail: yoanhealmeyda1209@gmail.com

C. F. Sánchez-Valdés
e-mail: cesar.sanchez@uacj.mx

1 Introduction

Several investigations in biomechanics have shown that models related to Cosserat-type media better capture the actual response of biological tissues (Eringen 1968; Cowin 1970; Yang and Lakes 1981, 1982; Lakes et al. 1990). The micromechanical study in Cosserat's media has had an impact on the mechanics of bones (Park and Lakes 1987; Lakes 1993; Tanaka and Adachi 1999; Fatemi et al. 2002, 2003; Goda et al. 1990; Jasiuk 2018), cardiac tissues (Sack et al. 2016; Hussan et al. 2012), etc.

The applicability of laminated structures in various branches of industry is well known. The investigation of their properties is important to improve and design new materials. There are micromechanical methods based on multiscale homogenization schemes that provide information about the properties of heterogeneous laminated micropolar or Cosserat media, for example: Properties of micropolar multi-layered media have been calculated using the finite element technique (Adhikary and Dyskin 1997; Riahi and Curran 2009; Lebée and Sab 2010). In these works, the potentiality of the Cosserat continuum model to predict the mechanical behavior of layered structures is analyzed. Moreover, the Cosserat continuums with 2D and 3D layered-like microstructure are analyzed by a finite element scheme in Riahi and Curran (2009, 2010). On the other hand, multiscale homogenization approaches applied to micropolar heterogeneous structures have been carried out by Nika (2022); Bigoni and Drugan (2007); Forest and Sab (1998); Forest et al. (2001); Forest and Trinh (2011); Gorbachev and Emel'yanov (2014, 2021), among others. In these approaches, the generalized stress and strain are linked to the displacements, strains, and stresses defined in the representative volume element.

Different works address the imperfect interface effects on multi-laminated media through the linear spring interface with zero thickness and the interphase models, (Bövik 1994; Ensan et al. 2003; Duong et al. 2011; Sertse and Yu 2017; Khoroshun 2019; Brito-Santana et al. 2019), among others. In the framework of heterogeneous

J. A. Otero
Escuela de Ingeniería y Ciencias, Tecnológico de Monterrey, Carr. al Lago de Guadalupe Km. 3.5, Estado de México 52926, Mexico
e-mail: j.a.otero@tec.mx

F. Lebon
Laboratoire de Mecanique et d'Acoustique, Universite Aix-Marseille, CNRS, Centrale Marseille,, CS 40006 13453 Marseille Cedex 13, France
e-mail: lebon@lma.cnrs-mrs.fr

R. Rizzoni
Department of Engineering, University of Ferrara, Via Saragat 1, 44122 Ferrara, Italy

M. Serpilli
Department of Civil and Building Engineering, and Architecture, Universitá Politecnica delle Marche, Via Brecce Bianche, 60131 Ancona, Italy

S. Dumont
University of Nîmes, Place Gabriel Péri, 30000 Nîmes, France
e-mail: serge.dumont@unimes.fr

micropolar or Cosserat elastic media, the problem of the existence of an imperfect interface between two contiguous phases has been considered. For example, the imperfect interface model applied to elastic composites (Achenbach and Zhu 1989; Hashin 2002) is generalized to micropolar media assuming that the couple tractions are continuous across the interface and proportional to the jumps of the out-of-plane microrotation (Videla and Atroshchenko 2017). In addition, the boundary element method is used to simulate microstructured Cosserat media with both perfect and uniform imperfect interfaces. The asymptotic analysis (see, for example, Ciarlet 1997) has proven to be a powerful mathematical tool to derive simplified models for thin films and structures (Geymonat et al. 2014; Serpilli et al. 2013). This technique has also been extensively used to study the mechanical behavior of layered composites, constituted by two solids bonded together by a thin interphase, considering different continuum theories with microstructure, such as micropolar elasticity (Serpilli 2018), poroelasticity (Serpilli 2019), and flexoelectricity (Serpilli et al. 2022). Recently, the effective behavior of multi-laminated micropolar composites is studied using the asymptotic homogenization method (Yanes et al. 2022; Rodríguez-Ramos et al. 2022). In both works, centro-symmetric cubic or isotropic constituents and perfect interface conditions are assumed. Other previous works dealing with the problem of imperfection in micropolar structures can be found in Rubin and Benveniste (2004); Dong et al. (2014, 2015); Kumari et al. (2022). Therefore, further analyses are required on this topic.

In the present work, based on the methodology presented in Yanes et al. (2022); Rodríguez-Ramos et al. (2022); Espinosa-Almeyda et al. (2022), the main results derived by the asymptotic homogenization method (AHM) to compute the effective engineering moduli for a laminated micropolar centro-symmetric composite are summarized, in which the interface between the layer phases is considered imperfect spring type. The layers are considered with isotropic symmetry. The imperfection is considered non-uniform and as a particular case uniform, controlled by different imperfection parameters and the cell length in the y_3-direction. The analytical expressions of the effective engineering moduli associated with the stiffness and torque are given as a function of the non-uniform imperfect parameters. An analysis of the behavior of the effective engineering coefficients depending on the imperfection is performed. The influence of the imperfection and the cell length in the direction of the imperfection is observed.

F. J. Sabina
Instituto de Investigaciones en matemáticas Aplicadas y Sistemas, Universidad Nacional Autónoma de México, Apartado Postal 20-126, Alcaldía Álvaro Obregón, 01000 CDMX, Mexico
e-mail: fjs@mym.iimas.unam.mx

2 Heterogeneous Problem Statement and Fundamental Equations

A periodic centro-symmetric linear elastic micropolar continuum Ω at the Cartesian coordinate system $\boldsymbol{x} = \{x_1, x_2, x_3\} \subset \mathbb{R}^3$ is defined by two independent sets of degrees of freedom given by the displacement $u_m(\boldsymbol{x})$ [m] and the microrotation $\omega_s(\boldsymbol{x})$ fields associated with each material point (Eringen 1999). For the static case, it is formulated by the linear and angular balance equations

$$\begin{aligned} \big(C_{ijmn}(\boldsymbol{x})\ e_{nm}(\boldsymbol{x})\big)_{,j} + f_i(\boldsymbol{x}) = 0, \\ \big(D_{ijmn}(\boldsymbol{x})\ \psi_{nm}(\boldsymbol{x})\big)_{,j} + \epsilon_{ijk}\big(C_{kjmn}(\boldsymbol{x})\ e_{nm}(\boldsymbol{x})\big) + g_i(\boldsymbol{x}) = 0, \end{aligned} \tag{19.1}$$

where $C_{ijmn}(\boldsymbol{x})$ [N/m^2] is the stiffness tensor, $D_{ijmn}(\boldsymbol{x})$ [N] is the torque tensor, $f_i(\boldsymbol{x})$ [N/m^3] are the body forces, and $g_i(\boldsymbol{x})$ [N/m^2] are the body couples functions, with $i, j, k, m, n, s = 1, 2, 3$. The micropolar strain $e_{mn}(\boldsymbol{x})$ and the torsion-curvature $\psi_{mn}(\boldsymbol{x})$ [m^{-1}] tensors are given by

$$e_{nm}(\boldsymbol{x}) = u_{m,n}(\boldsymbol{x}) + \epsilon_{mns}\omega_s(\boldsymbol{x}), \quad \psi_{nm}(\boldsymbol{x}) = \omega_{m,n}(\boldsymbol{x}), \tag{19.2}$$

where ϵ_{mns} is the Levi-Civita tensor, u_m is the displacement vector, and ω_m is the microrotation vector, independent of the displacement. The notation $f_{,m} \equiv \partial f/\partial x_m$ and the square brackets contain the physical units of measure for the variable. In Eqs. (19.1) and (19.2), the symmetric part of $e_{mn}(\boldsymbol{x})$ corresponds to the classical strain tensor, whereas its skew-symmetric part accounts for the local reorientation of the microstructure. Also, the symmetry conditions $C_{ijmn}(\boldsymbol{x}) = C_{mnij}(\boldsymbol{x})$ and $D_{ijmn}(\boldsymbol{x}) = D_{mnij}(\boldsymbol{x})$ are satisfied.

The system, Eq. (19.1), together with the boundary conditions on $\partial\Omega$

$$\begin{aligned} u_m(\boldsymbol{x})\ |_{\partial\Omega_1} = 0, \quad \big(C_{ijmn}(\boldsymbol{x})\, e_{nm}(\boldsymbol{x})\big)n_j\ |_{\partial\Omega_2} = F_i(\boldsymbol{x}), \\ \omega_m(\boldsymbol{x})\ |_{\partial\Omega_3} = 0, \quad \big(D_{ijmn}(\boldsymbol{x})\, \psi_{nm}(\boldsymbol{x})\big)n_j\ |_{\partial\Omega_4} = G_i(\boldsymbol{x}), \end{aligned} \tag{19.3}$$

where $F_i(\boldsymbol{x})$ and $G_i(\boldsymbol{x})$ are the surface body forces and moments, representing the static boundary value problem associated with the linear theory of micropolar elasticity whose coefficients are rapidly oscillating. In Eq. (19.3), n_j is the unit outer normal vector to $\partial\Omega$ and the subsets $\partial\Omega_i$ satisfy $\partial\Omega_i \bigcap\limits_{i\neq j} \partial\Omega_j \neq \varnothing$ (disjoint sets) and $\partial\Omega = \bigcup\limits_{i=1}^{4} \partial\Omega_i$.

In addition to the problem statement (Eqs. (19.1)–(19.3)), we deal with the spring model described above considering imperfect contact conditions at the interface Γ, such as

$$\begin{aligned}\left(C_{ijmn}(x)e_{nm}(x)\right)n_j &= K_{ij}\left[\!\left[u_j\right]\!\right],\ \left[\!\left[\left(C_{ijmn}(x)e_{nm}(x)\right)n_j\right]\!\right] = 0,\ \text{on}\ \Gamma\\ \left(D_{ijmn}(x)\psi_{nm}(x)\right)n_j &= Q_{ij}\left[\!\left[\omega_j\right]\!\right],\ \left[\!\left[\left(D_{ijmn}(x)\psi_{nm}(x)\right)n_j\right]\!\right] = 0,\ \text{on}\ \Gamma\end{aligned} \tag{19.4}$$

where $[\![p]\!] = p^{(1)} - p^{(2)}$ means the jump of the function p across the interface Γ. K_{ij} [N/m^3] and Q_{ij} [N/m] are the extensional and microtational imperfection parameters, such that $K_{ij} = \begin{pmatrix} K_t & 0 & 0 \\ 0 & K_s & 0 \\ 0 & 0 & K_n \end{pmatrix}$ and $Q_{ij} = \begin{pmatrix} Q_t & 0 & 0 \\ 0 & Q_s & 0 \\ 0 & 0 & Q_n \end{pmatrix}$. Here, K_t, K_s, K_n, Q_t, Q_s, and Q_n are the interface parameters in the normal and tangential directions, which are considered equals for the sake of simplicity as follows: $K_t = K_s = K_n$ and $Q_t = Q_s = Q_n$. An equivalent form of the imperfect contact conditions (19.4) has been derived for soft micropolar interfaces in Serpilli (2018), by means of the asymptotic analysis.

3 Asymptotic Homogenization Method and Effective Engineering Moduli for Periodic Laminated Micropolar Media

From now on, let us consider that the three-dimensional heterogeneous centrosymmetric linear elastic micropolar continuum Ω is described by a parallelepiped of dimensions l_i $(i = 1, 2, 3)$ generated by repetitions of a periodic cell Y, whose layered direction is along the y_3-axis. At the microscale, the transversal cross-section of Y is characterized by a bi-laminated composite in the plane Oy_2y_3, see Fig. 19.1, where the constituent material phases are denoted by S_γ $(\gamma = 1, 2)$ with volume V_γ, such as $\mathrm{Y} = S_1 \cup S_2$, $S_1 \cap S_2 = \emptyset$, and $\mathrm{V}_1 + \mathrm{V}_2 = 1$. Imperfect contact conditions

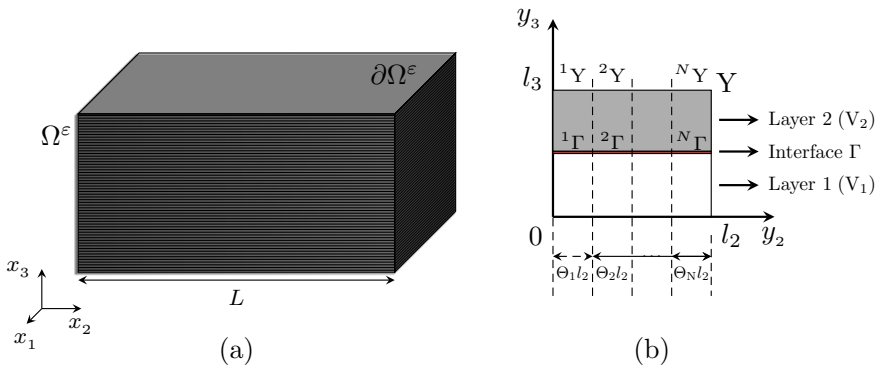

Fig. 19.1 **a** Heterogeneous Cosserat composite; **b** Cross-section of a periodic bi-laminated structure Y at the plane Oy_2y_3 with non-uniform imperfect interface Γ partitioned in N disjoint sub-interfaces ${}^r\Gamma$ $(r = 1, 2, \ldots, N)$

(uniform or non-uniform) are assumed at the interface region Γ between the layers following Eq. (19.4).

The non-uniform imperfect interface is defined by partitioning Γ along the y_2 direction, where $\theta_r\ \ell_2$ is the length of the r-partition (denoted by ${}^r\Gamma$) with imperfection length fraction θ_r $(r = 1, \ldots, N)$, ℓ_2 is the characteristic length of Y along the y_2 direction, and N is the number of partitions, such as $\Gamma = \bigcup_{r=1}^{N} {}^r\Gamma$. In this context, K_{ij} and Q_{ij} are considered piecewise linear functions in each unit cell partition ${}^r\mathrm{Y}$ (with r fixed), such as ${}^r\mathrm{Y} = \left\{\mathbf{y} \in \mathbb{R}^3 : 0 < y_i < \ell_i, \text{ and } \sum_{s=0}^{r-1} \theta_s \ell_2 < y_2 < \sum_{s=1}^{r} \theta_s \ell_2,\ \theta_0 = 0\right\}$ and $\mathrm{Y} = \bigcup_{r=1}^{N} {}^r\mathrm{Y}$. Also, ${}^r\mathrm{f} = \begin{cases} {}^1\mathrm{f} \text{ in } {}^1\mathrm{Y} \\ \vdots \\ {}^N\mathrm{f} \text{ in } {}^N\mathrm{Y} \end{cases}$, where f might be replaced by K_{ij} and Q_{ij} or any function defined in ${}^r\mathrm{Y}$. On the other hand, as a particular case, a uniform interface is taken into account when the values of the imperfection parameters in each cell partition ${}^r\mathrm{Y}$ are equal.

In this framework, the applied methodology based on the AHM for centrosymmetric micropolar composites with perfect contact conditions (Yanes et al. 2022; Rodríguez-Ramos et al. 2022) is implemented in the case of an imperfect interface. The AHM provides averaged expressions for the rapidly oscillating elasticity tensors of the original problem and proposes a homogeneous equivalent medium with the same behavior. Its main assumptions are that all fields are considered as power series of the small and positive definite dimensionless parameter ε whose coefficients are dependent on the macro $(\boldsymbol{x})$ and micro $(\boldsymbol{y})$ scales; see, for instance, (Sanchez-Palencia 1980; Pobedrya 1984; Bakhvalov and Panasenko 1989). Both scales are related as $\boldsymbol{y} = \boldsymbol{x}/\varepsilon$, where $\varepsilon = \ell/L \ll 1$ is defined by the ratio between the characteristic size of the periodicity cell (ℓ) and the diameter of the body (L).

The AHM starts from the substitution of the expansions for the displacements $u_m^{\varepsilon}(\boldsymbol{x})$ and the microrotations $\omega_m^{\varepsilon}(\boldsymbol{x})$

$$u_m^{\varepsilon}(\boldsymbol{x}) = \sum_{\alpha=0}^{\infty} \varepsilon^{\alpha} u_m^{(\alpha)}(\boldsymbol{x}, \boldsymbol{y}), \quad \omega_m^{\varepsilon}(\boldsymbol{x}) = \sum_{\alpha=0}^{\infty} \varepsilon^{\alpha} \omega_m^{(\alpha)}(\boldsymbol{x}, \boldsymbol{y}), \tag{19.5}$$

into the problem (Eqs. 19.1–19.4), and following algebraic operations and differentiation rules. Here, $u_m^{(i)}(\boldsymbol{x}, \boldsymbol{y})$ and $\omega_m^{(i)}(\boldsymbol{x}, \boldsymbol{y})$ $(i = 0, 1, 2, \ldots)$ are infinitely differentiable and Y-periodic functions with respect to $\boldsymbol{y}$. Thus, a sequence of problems given by partial differential equations is obtained in relation to the power of the ε parameter. From them, the formulation of local problems on Y, the effective moduli, and the equivalent homogenized problem with its asymptotic solution are obtained. Details about the AHM methodology related to micropolar laminated composites are shown in Forest et al. (2001), Gorbachev and Emel'yanov (2014), Yanes et al. (2022), Rodríguez-Ramos et al. (2022) and are omitted here.

The mathematical statement of the ${}_{pq}{}^r\mathcal{L}^1$ and ${}_{pq}{}^r\mathcal{L}^2$ (with $p, q = 1, 2, 3$) local problems over each partition ${}^r\mathrm{Y}$ are given by

$$
{}^{r}_{pq}\mathcal{L}^{1}\begin{cases}\left(C_{i3pq}+C_{i3m3}{}^{r}_{pq}N'_{m}\right)'=0,\ \text{in}\,{}^{r}\mathrm{Y}\\ \left[\!\left[C_{i3pq}+C_{i3m3}{}^{r}_{pq}N'_{m}\right]\!\right]n_3=0,\ \text{in}\,{}^{r}\Gamma\\ \left(C_{i3pq}+C_{i3m3}{}^{r}_{pq}N'_{m}\right)n_3={}^{r}K_{ij}\left[\!\left[{}^{r}_{pq}N_{j}\right]\!\right],\ \text{in}\,{}^{r}\Gamma\\ \left\langle {}^{r}_{pq}N_{m}\right\rangle_{{}^{r}Y}=0,\end{cases}
\tag{19.6}
$$

$$
{}^{r}_{pq}\mathcal{L}^{2}\begin{cases}\left(D_{i3pq}+D_{i3m3}{}^{r}_{pq}M'_{m}\right)'=0,\ \text{in}\,{}^{r}\mathrm{Y}\\ \left[\!\left[D_{i3pq}+D_{i3m3}{}^{r}_{pq}M'_{m}\right]\!\right]n_3=0,\ \text{in}\,{}^{r}\Gamma\\ \left(D_{i3pq}+D_{i3m3}{}^{r}_{pq}M'_{m}\right)n_3={}^{r}Q_{ij}\left[\!\left[{}^{r}_{pq}M_{j}\right]\!\right],\ \text{in}\,{}^{r}\Gamma\\ \left\langle {}^{r}_{pq}M_{m}\right\rangle_{{}^{r}Y}=0,\end{cases}
\tag{19.7}
$$

where $(\bullet)'=\mathrm{d}(\bullet)/\mathrm{d}y_3$. In Eqs. (19.6) and (19.7), ${}^{r}_{pq}N_m$ and ${}^{r}_{pq}M_m$ are the local pq-displacements and pq-microrotations defined in the r-partition of the cell Y, respectively. The periodicity conditions ${}_{pq}N_m(0)={}_{pq}N_m(l_i)$ and ${}_{pq}M_m(0)={}_{pq}M_m(l_i)$ are satisfied and the unknown functions ${}^{r}_{pq}N_m$ and ${}^{r}_{pq}M_m$ only depend on y_3 as well. The symbol $\langle p\rangle$ denotes Voigt's average of the property p, i.e. $\langle p\rangle=\sum_{i=1}^{N}p^{(i)}\mathrm{V}_i$ with N the number of phases in Y and $\sum_{i=1}^{N}\mathrm{V_i}=1$. In case of a bi-laminated composite, $\langle p\rangle=p^{(1)}\mathrm{V}_1+p^{(2)}\mathrm{V}_2$ where $\mathrm{V}_1=\gamma/\ell_3$ and $\mathrm{V}_2=1-\gamma/\ell_3$ are the volume fractions per unit length occupied by layers 1 and 2, respectively, such as $\mathrm{V}_1+\mathrm{V}_2=1$. γ is the y_3 coordinate of the constituent contact.

Once the unknown functions ${}^{r}_{pq}N_m$ and ${}^{r}_{pq}N_m$ are determined, the corresponding effective properties in terms of the r-interface-partition formulation can be found as follows:

$$
C^{*}_{ijpq}=\sum_{r=0}^{N}\theta_r\left\langle C_{ijpq}+C_{ijm3}{}^{r}_{pq}N'_{m}\right\rangle_{{}^{r}\mathrm{Y}},
\tag{19.8}
$$

$$
D^{*}_{ijpq}=\sum_{r=0}^{N}\theta_r\left\langle D_{ijpq}+D_{ijm3}{}^{r}_{pq}M'_{m}\right\rangle_{{}^{r}\mathrm{Y}}.
\tag{19.9}
$$

The local functions ${}^{r}_{pq}N'_m$ and ${}^{r}_{pq}M'_m$ can be determined as it is shown in Yanes et al. (2022), Rodríguez-Ramos et al. (2022) and after their replacement into Eq. (19.8), the corresponding stiffness and torque effective properties are obtained as functions of the constituent's properties, the imperfection parameters, and the constituent's volume fractions

$$
\begin{gathered}
C^{*}_{ijpq}=\left\langle C_{ijpq}-C_{ijm3}C^{-1}_{m3a3}C_{a3pq}\right\rangle+\\
\textstyle\sum_{r=1}^{N}\theta_r\left\langle C_{ijm3}C^{-1}_{m3a3}\right\rangle\left(\left\langle C^{-1}_{a3b3}\right\rangle+\ell_3^{-1}\,{}^{r}K^{-1}_{ab}\right)^{-1}\left\langle C^{-1}_{b3c3}C_{c3pq}\right\rangle,
\end{gathered}
\tag{19.10}
$$

$$
\begin{gathered}
D^{*}_{ijpq}=\left\langle D_{ijpq}-D_{ijm3}D^{-1}_{m3a3}D_{a3pq}\right\rangle+\\
\textstyle\sum_{r=1}^{N}\theta_r\left\langle D_{ijm3}D^{-1}_{m3a3}\right\rangle\left(\left\langle D^{-1}_{a3b3}\right\rangle+\ell_3^{-1}\,{}^{r}Q^{-1}_{ab}\right)^{-1}\left\langle D^{-1}_{b3c3}D_{c3pq}\right\rangle.
\end{gathered}
\tag{19.11}
$$

Since both local problems (Eqs. 19.6 and 19.7) and the effective properties (Eqs. 19.10 and 19.11) have the same structure, only the analytical expressions for the stiffness are shown. The analytical expressions for effective torque moduli can be found replacing D for C, and Q for K.

3.1 Effective Engineering Moduli

Assuming that the constituents are centro-symmetric isotropic materials, these are characterized by 6 independent constants $C_{1122}, C_{1212}, C_{1221}, D_{1122}, D_{1212}$, and D_{1221}, see Hassanpour and Heppler (2017), through the relations

$$C_{ijmn} = C_{1122}\delta_{ij}\delta_{mn} + C_{1212}\delta_{im}\delta_{jn} + C_{1221}\delta_{in}\delta_{jm}, \tag{19.12}$$

$$D_{ijmn} = D_{1122}\delta_{ij}\delta_{mn} + D_{1212}\delta_{m}\delta_{jn} + D_{1221}\delta_{in}\delta_{jm}, \tag{19.13}$$

where δ_{ij} is the Kronecker delta tensor.

The global symmetry after the homogenization process is orthotropic, defined by 18 non-zero effective moduli, as it is pointed out in Yanes et al. (2022), Rodríguez-Ramos et al. (2022). The nine non-zero stiffness effective properties are $C^*_{1111} = C^*_{2222}$, C^*_{3333}, C^*_{1122}, $C^*_{1133} = C^*_{2233}$, $C^*_{1313} = C^*_{2323}$, $C^*_{3232} = C^*_{3131}$, $C^*_{1331} = C^*_{2332}$, $C^*_{1212} = C^*_{2121}$, and C^*_{1221}. Similarly, the other nine torque properties can be derived.

Following the strain-stress relationships for a centro-symmetric micropolar media according to Eq. (19.1), and applying the effective relations reported in Eqs. (64)–(66) of (Rodríguez-Ramos et al. 2022) for the corresponding stiffness effective properties (see, Eq. 19.10), the independent effective engineering moduli written as functions of the stiffness matrix components and the imperfection parameters are given as follows:

Effective Young's moduli:

$$\begin{aligned} {}_sE^*_1 = {}_sE^*_2 &= \frac{\Big(\langle C_{1111}\rangle - \langle C_{1122}\rangle\Big)\Big(\langle C_{1111}\rangle + \langle C_{1122}\rangle - 2\big\langle C^2_{1122}\, C^{-1}_{1111}\big\rangle\Big)}{\langle C_{1111}\rangle - \big\langle C^2_{1122}\, C^{-1}_{1111}\big\rangle}, \\ {}_sE^*_3 &= \frac{\Big(\langle C_{1111}\rangle + \langle C_{1122}\rangle - 2\big\langle C^2_{1122} C^{-1}_{1111}\big\rangle\Big)\, B_1({}^rK_{33})}{\langle C_{1111}\rangle + \langle C_{1122}\rangle - 2\big\langle C^2_{1122} C^{-1}_{1111}\big\rangle + 2\big\langle C_{1122} C^{-1}_{1111}\big\rangle^2\, B_1({}^rK_{33})}. \end{aligned} \tag{19.14}$$

Effective shear moduli:

$$
\begin{aligned}
{}_{S}G_{12}^{*} = {}_{S}G_{21}^{*} &= \frac{\langle C_{1212}\rangle^{2} - \langle C_{1221}\rangle^{2}}{\langle C_{1212}\rangle}, \\
{}_{S}G_{13}^{*} = {}_{S}G_{23}^{*} &= \frac{\Big(\langle C_{1212}\rangle - \big\langle C_{1221}^{2}C_{1212}^{-1}\big\rangle\Big)\, B_{2}({}^{r}K_{22})}{\langle C_{1212}\rangle - \big\langle C_{1221}^{2}C_{1212}^{-1}\big\rangle + \big\langle C_{1221}C_{1212}^{-1}\big\rangle^{2}\, B_{2}({}^{r}K_{22})}, \\
{}_{S}G_{32}^{*} = {}_{S}G_{31}^{*} &= \langle C_{1212}\rangle - \big\langle C_{1221}^{2}C_{1212}^{-1}\big\rangle .
\end{aligned}
\tag{19.15}
$$

Effective Poisson's ratios:

$$
\begin{aligned}
{}_{S}\nu_{21}^{*} &= \frac{\big\langle C_{1122}^{2}C_{1111}^{-1}\big\rangle - \langle C_{1122}\rangle}{\big\langle C_{1122}^{2}C_{1111}^{-1}\big\rangle - \langle C_{1111}\rangle}, \\
{}_{S}\nu_{32}^{*} = {}_{S}\nu_{31}^{*} &= \frac{\big\langle C_{1122}C_{1111}^{-1}\big\rangle\, B_{1}({}^{r}K_{33})}{\langle C_{1111}\rangle + \langle C_{1122}\rangle - 2\big\langle C_{1122}^{2}C_{1111}^{-1}\big\rangle + 2\big\langle C_{1122}C_{1111}^{-1}\big\rangle^{2}\, B_{1}({}^{r}K_{33})}.
\end{aligned}
\tag{19.16}
$$

Effective shear-strain ratios:

$$
{}_{S}\zeta_{2112}^{*} = \frac{\langle C_{1221}\rangle}{\langle C_{1212}\rangle}, \qquad {}_{S}\zeta_{3223}^{*} = \big\langle C_{1221}C_{1212}^{-1}\big\rangle , \tag{19.17}
$$

where the following parameters $B_{1}({}^{r}K_{33})$ and $B_{2}({}^{r}K_{22})$ are introduced for better presentation of the formulae

$$
\begin{aligned}
B_{1}({}^{r}K_{33}) &= \sum_{r=1}^{N} \theta_{r}\Big(\big\langle C_{1111}^{-1}\big\rangle + \frac{1}{\ell_{3}}\,{}^{r}K_{33}^{-1}\Big)^{-1}, \\
B_{2}({}^{r}K_{22}) &= \sum_{r=1}^{N} \theta_{r}\Big(\big\langle C_{1212}^{-1}\big\rangle + \frac{1}{\ell_{3}}\,{}^{r}K_{22}^{-1}\Big)^{-1}.
\end{aligned}
\tag{19.18}
$$

The effective engineering constants for torque moduli can be written in the analogous form, and they are denoted by a subscript T, for example: the torsional Young's moduli ${}_{T}E_{i}^{*}$, the torsional shear moduli ${}_{T}G_{12}^{*}$, ${}_{T}G_{13}^{*}$ and ${}_{T}G_{32}^{*}$, the twist Poisson's coefficient ${}_{T}\nu_{21}^{*}$ and ${}_{T}\nu_{32}^{*}$, and the twist shear-strain ratios ${}_{S}\zeta_{2112}^{*}$ and ${}_{S}\zeta_{3223}^{*}$.

4 Numerical Results

In this section, Eqs. (19.14)–(19.18) are implemented to analyze the effect of a non-uniform or uniform imperfect interface Γ on the effective engineering moduli of a centro-symmetric bi-laminated Cosserat composite (layer 1/layer 2 = SyF/PUF) with isotropic constituents. The values of the Cosserat elastic parameters listed in Table 19.1 are used for computations through the relations $C_{1122} \equiv \lambda$, $(C_{1212} + C_{1221})/2 \equiv \mu$, $(C_{1212} - C_{1221})/2 \equiv \alpha$, $D_{1122} \equiv \beta$, $(D_{1212} + D_{1221})/2 \equiv$

Table 19.1 Constituent material properties. [a] Syntactic foam—hollow glass spheres in epoxy resin, and [b] Dense polyurethane foam

Material properties	λ (MPa)	μ (MPa)	α (MPa)	β (N)	γ (N)	ϵ (N)
SyF[a]	2097.0	1033.0	114.8	−2.91	4.364	−0.133
PUF[b]	762.7	104.0	4.333	−26.65	39.98	4.504

γ, and $(D_{1212} - D_{1221})/2 \equiv \epsilon$, where λ and μ are the Lamé parameters, α is the micropolar couple modulus, and the properties β, γ, and ϵ represent the additional micropolar elastic constants introduced in micropolar theory, according to the following constitutive law for a micropolar isotropic centro-symmetric material:

$$\begin{aligned} \sigma_{ij} &= (\mu + \kappa)e_{ij} + (\mu - \kappa)e_{ji} + \lambda e_{kk}\delta_{ij}, \\ \chi_{ij} &= (\gamma + \beta)\psi_{ij} + (\gamma - \beta)\psi_{ji} + \alpha\psi_{kk}\delta_{ij}, \end{aligned} \tag{19.19}$$

where σ_{ij} and χ_{ij} represent the stress and couple-stress tensor components, respectively. These material data are taken from Hassanpour and Heppler (2017). For the micropolar constants, the same notation of (Hassanpour and Heppler 2017) is used, where α is κ, β is α, γ remains γ, and ϵ is β.

4.1 Non-uniform Imperfect Interface

Here, the non-uniform imperfect interface Γ is defined by a partition of N disjoint sub-interfaces ${}^r\Gamma$ characterized by an imperfection length fraction ${}^r\theta$ and by two sets of imperfection parameters (${}^rK_{ij}$ and ${}^rQ_{ij}$) with a considerably large gap between their values for each partition; see Sect. 19.3.

In Table 19.3, the effective engineering moduli related to the stiffness $\left({}_SE_3^*,\ {}_SG_{13}^*,\ {}_S\nu_{31}^*\right)$ and torques $\left({}_TE_3^*,\ {}_TG_{13}^*,\ {}_T\nu_{31}^*\right)$ affected by the imperfection are shown for four SyF volume fractions (V_1) equal to 0.2, 0.4, 0.6, and 0.8. Two different partitions of Γ are analyzed, one with $N = 2$ partitions and another with $N = 4$

Table 19.2 Sets of values for the ${}^rK_{ij}$ and ${}^rQ_{ij}$ imperfection parameters considered in each partition of ${}^r\Gamma$

	$N = 2$				$N = 4$							
Set	${}^1K_{ij}$	${}^2K_{ij}$	${}^1Q_{ij}$	${}^2Q_{ij}$	${}^1K_{ij}$	${}^2K_{ij}$	${}^3K_{ij}$	${}^4K_{ij}$	${}^1Q_{ij}$	${}^2Q_{ij}$	${}^3Q_{ij}$	${}^4Q_{ij}$
S_1	10^3	10^4	10^1	10^2	10^3	10^4	10^5	10^6	10^1	10^2	10^3	10^4
S_2	10^5	10^6	10^3	10^4	10^5	10^6	10^7	10^8	10^3	10^4	10^5	10^6
S_3	10^7	10^8	10^5	10^6	10^7	10^8	10^9	10^{10}	10^5	10^6	10^7	10^8

Table 19.3 Variation of the effective engineering moduli related to non-uniform imperfect interface for four SyF volume fractions (V_1). The moduli ${}_S E_3^*$, ${}_S G_{13}^*$ are measured in [MPa]; ${}_T E_3^*$, ${}_T G_{13}^*$ in [N]; ${}_S \nu_{31}^*$, ${}_T \nu_{31}^*$ are dimensionless

Moduli	V_1	$N = 2$			$N = 4$			Perfect
		S_1	S_2	S_3	S_1	S_2	S_3	
${}_S E_3^*$	0.2	0.0055*	0.5493	48.8405	0.2774	25.1987	307.7864	581.9802
	0.4	0.0055*	0.5495	50.4403	0.2775	25.7829	392.7140	853.5091
	0.6	0.0055*	0.5496	51.5785	0.2776	26.2485	489.5963	1194.0030
	0.8	0.0055*	0.5497	52.5544	0.2776	26.6766	626.0288	1719.9066
${}_S G_{13}^*$	0.2	0.0055*	0.5437	25.9370	0.2752	14.7569	47.3517	62.7962
	0.4	0.0055*	0.5457	31.2829	0.2759	17.0148	67.8537	97.8025
	0.6	0.0055*	0.5470	35.9172	0.2765	19.1634	92.8556	142.0619
	0.8	0.0055*	0.5481	41.0084	0.2770	21.6470	135.7580	218.5210
${}_S \nu_{32}^*$	0.2	3.2×10^{-6}	3.2×10^{-4}	0.0283	2×10^{-4}	0.0146	0.1785	0.3376
	0.4	1.9×10^{-6}	1.9×10^{-4}	0.0171	9×10^{-5}	0.0088	0.1335	0.2901
	0.6	1.3×10^{-6}	1.3×10^{-4}	0.0118	6×10^{-5}	0.0060	0.1117	0.2724
	0.8	0.9×10^{-6}	0.9×10^{-5}	0.0086	5×10^{-5}	0.0044	0.1024	0.2813
${}_T E_3^*$	0.2	6×10^{-5}*	0.0044	0.0219	0.0025	0.0210	0.0227	0.0228
	0.4	6×10^{-5}*	0.0041	0.0151	0.0024	0.0147	0.0155	0.0156
	0.6	6×10^{-5}*	0.0033	0.0083	0.0021	0.0081	0.0084	0.0084
	0.8	5×10^{-5}*	0.0010	0.0012	0.0008	0.0012	0.0012	0.0012
${}_T G_{13}^*$	0.2	6×10^{-5}*	0.0055*	0.5043	0.0028*	0.2585	3.9585	8.2248
	0.4	6×10^{-5}*	0.0055*	0.4800	0.0028*	0.2477	2.7316	5.1540
	0.6	6×10^{-5}*	0.0055*	0.4512	0.0028*	0.2360	1.9728	3.3367
	0.8	6×10^{-5}*	0.0055*	0.3998	0.0028*	0.2179	1.2555	1.7927
${}_T \nu_{32}^*$	0.2	−0.0024	−0.1943	−0.9585	−0.1085	−0.9211	−0.9964	−0.9990
	0.4	−0.0035	−0.2605	−0.9704	−0.1511	−0.9432	−0.9965	−0.9987
	0.6	−0.0065	−0.3955	−0.9833	−0.2483	−0.9677	−0.9975	−0.9989
	0.8	−0.0439	−0.8207	−0.9973	−0.6981	−0.9949	−0.9994	−0.9996

* The values with more significant digits are given in Appendix A

partitions. In the case of $N = 2$, $\theta_1 = \theta_2 = 0.5$ and the corresponding imperfection parameters are defined by ${}^r K_{ij}$ and ${}^r Q_{ij}$ $(r = 1, 2)$, whereas, for $N = 4$, $\theta_1 = \theta_2 = \theta_3 = \theta_4 = 0.25$ and the imperfection parameters are ${}^r K_{ij}$ and ${}^r Q_{ij}$ $(r = 1, \ldots, 4)$ with $ij = 22, 33$. For both partitions, three different sets of imperfection parameters (S_1, S_2 and S_3) are considered for ${}^r K_{ij}$ and ${}^r Q_{ij}$; see Table 19.2. For example, when $N = 2$, S_1 is the set of values ${}^1 K_{ij} = 10^{-1}$, ${}^2 K_{ij} = 10^0$, ${}^1 Q_{ij} = 10^{-1}$, and ${}^2 Q_{ij} = 10^0$. The remaining sets can be understood in a similar form. The characteristic lengths of Y along the x_2 and x_3 directions are $\ell_3 = 10^{-6}$m and $\ell_2 = 1$, respectively. In addition, the effective values associate with the perfect contact case are reported for the same volume fractions.

From Table 19.3, it can be observed that the influence of the non-uniform imperfect interface is remarkable in the effective engineering properties, regardless of the V_1 volume fraction, and even the microstructure of the imperfection region determined by the partition N affects the behavior of the properties. A non-uniform interface with values for ${}^r K_{ij}$ and ${}^r Q_{ij}$ as in S_1 or lower implies the delamination of the

material, and, hence, a loss of the effective properties. However, as the values of the imperfection parameters increase as in S_2 and S_3, an approach to the existence of a perfect interface is appreciated, and then the engineering moduli have an increment. The perfect contact is reached when the values of ${}^{r}K_{ij}$ and ${}^{r}Q_{ij}$ parameters are 10^{14} in each ${}^{r}\Gamma$. The highest values of the engineering constants are achieved in this perfect case. Furthermore, it can be seen that the effect of the imperfection is more noticeable in the engineering moduli related to compliance $\left({}_{S}E_3^*,\ {}_{S}G_{13}^*,\ {}_{S}\nu_{31}^*\right)$ than those related to torque $\left({}_{T}E_3^*,\ {}_{T}G_{13}^*,\ {}_{T}\nu_{31}^*\right)$, and is even more pronounced for high SyF volume fraction. As N increases, the microstructure of the imperfection becomes finer, and its effect on the constant engineering behaviors is evident.

On the other hand, in Table 19.4, the remaining effective engineering moduli, which are independent of the imperfection effect, are reported for four SyF volume fractions ($V_1 = 0.2$, 0.4, 0.6, and 0.8). As can be seen in Eqs. (19.14)–(19.18), these effective moduli only depend on the material constituents and their volume fractions, therefore, their behaviors are related to the hardness or softness of the SyF material properties. According to Table 19.1, we can see that SyF is harder than PUF. Thus, for the perfect case, as V_1 volume fraction increases, the effective engineering constants ${}_{S}E_1^*$, ${}_{S}E_3^*$, ${}_{S}G_{13}^*$, ${}_{S}G_{12}^*$, and ${}_{S}G_{31}^*$ for compliance and the other ones ${}_{T}\zeta_{2112}^*$ and ${}_{T}\zeta_{3223}^*$ for torques increase too. The opposite happens for the remaining Cosserat elastic parameters, which are softer for SyF and thus for the composite as V_1 increases. The effective engineering constants are stiffer in this case.

4.2 Uniform Imperfect Interface

Now, the effect of a uniform imperfect interface on the effective engineering moduli is analyzed. The uniform imperfect interface is defined as a particular case of the previously described non-uniform imperfect ones assuming that the values of ${}^{r}K_{ij}$ and ${}^{r}Q_{ij}$ imperfection parameters are the same along Γ, such as $K \equiv {}^{r}K_{ij}$ and $Q \equiv {}^{r}Q_{ij}$.

The numerical simulations are conducted for different grades of imperfection, such that the values for K are 10^6, 5×10^6, 10^7, 3×10^7, 5×10^7, 10^8, and the latest 10^{10} (perfect contact); and for Q they are 10^5, 2×10^5, 3×10^5, 5×10^5, 10^6, 5×10^6, and finally 10^7 (perfect contact), respectively. Also, the characteristic lengths $\ell_3 = 10^{-4}$ and $\ell_2 = 1$.

In Figs. 19.2 and 19.3, only the behaviors of the effective engineering moduli affected by the imperfection are illustrated for a bi-laminated Cosserat composites (SyF/PUF) versus SyF volume fraction considering different imperfect parameters. We remark that these effective engineering moduli are sensitive to the imperfection, that is, they get weaker and only reach their highest values in the case of perfect contact. Notice that ${}_{S}E_3^*$, ${}_{S}G_{13}^*$, and ${}_{S}\nu_{32}^*$ are more sensitive to the imperfection K when V_1 increases, whereas ${}_{T}G_{13}^*$ and ${}_{T}\nu_{32}^*$ have the same performance for Q when low values of V_1 are attached. However, ${}_{T}E_3^*$ undergoes slight changes caused by the effect of the Q imperfection. In this sense, a zoom illustrates the slight weakening

Table 19.4 Effective engineering moduli calculated for four SyF volume fractions V_1. The moduli ${}_S E_1^*$, ${}_S G_{12}^*$, and ${}_S G_{31}^*$ are measured in [MPa]; ${}_T E_1^*$, ${}_T G_{12}^*$, and ${}_T G_{31}^*$ in [N]; and the others ${}_S \nu_{21}^*$, ${}_S \zeta_{2112}^*$, ${}_S \zeta_{3223}^*$, ${}_T \nu_{21}^*$, ${}_T \zeta_{2112}^*$, and ${}_T \zeta_{3223}^*$ are dimensionless

V_1	${}_S E_1^*$	${}_S G_{12}^*$	${}_S G_{31}^*$	${}_S \nu_{21}^*$	${}_S \zeta_{2112}^*$	${}_S \zeta_{3223}^*$
0.2	793.4487	96.8720	95.9654	0.3690	0.8329	0.8960
0.4	1285.0272	176.1125	175.2921	0.3510	0.8149	0.8720
0.6	1776.1720	255.2062	254.6187	0.3427	0.8071	0.8480
0.8	2267.1612	334.2504	333.9454	0.3380	0.8027	0.8240
V_1	${}_T E_1^*$	${}_T G_{12}^*$	${}_T G_{31}^*$	${}_T \nu_{21}^*$	${}_T \zeta_{2112}^*$	${}_T \zeta_{3223}^*$
0.2	0.0228	12.9020	12.8438	−0.9997	0.8037	0.8506
0.4	0.0156	9.6077	9.4956	−0.9997	0.8133	0.9036
0.6	0.0084	6.3040	6.1475	−0.9998	0.8306	0.9567
0.8	0.0012	2.9721	2.7994	−0.9999	0.8706	1.0098

of the property when V_1 is close to 0.4. Despite the imperfection effect, the ${}_S E_3^*$ and ${}_S G_{13}^*$ become stronger as V_1 increase, whereas the opposite occurs for ${}_T E_3^*$ and ${}_T G_{13}^*$.

On the other hand, the behavior of the effective Poisson ${}_S \nu_{32}^*$ and twist Poisson ${}_T \nu_{32}^*$ moduli is remarkable. The module ${}_S \nu_{32}^*$ has a concave upward behavior, whereas ${}_T \nu_{32}^*$ is concave downward for all ${}^r K_{ij}$ and ${}^r Q_{ij}$ imperfection parameters in the whole V_1 interval. Also, ${}_S \nu_{32}^*$ is positive and ${}_T \nu_{32}^*$ is negative. These behaviors are similar to the one reported by Dunn and Ledbetter (1995) for an elastic solid weakened by porosity and microcracks. Paraphrasing his statement 4 from the conclusions (Dunn and Ledbetter 1995), the Poisson and twist Poisson moduli can increase, decrease, or remain unchanged depending on the imperfection parameters and the SyF volume fractions. The trend of the pictures is reversed by passing from Figs. 19.2 and 19.3, they are mirror-like. This can be understood by looking at the values in Table 19.1; the elastic coefficients are larger for SyF, but the opposite happens for the micropolar constants—they are larger for PUF.

Notice the existence of a change correlation point for ${}_T \nu_{32}^*$ in $V_1 = 0.8333087$ (Fig. 19.3). This point is a consequence of $\langle D_{1111} \rangle + \langle D_{1122} \rangle - 2 \left\langle D_{1122}^2 D_{1111}^{-1} \right\rangle = 0$ in Eq. (19.16) for the torque. Thus, ${}_T \nu_{32}^* = {}_T \nu_{31}^* = 0.5 \left\langle D_{1122} D_{1111}^{-1} \right\rangle^{-1} \equiv H(V_1)$. All the curves are intercepted in this correlation point and $H(V_1)$ shows the independence of ${}_T \nu_{32}^*$ with respect to ${}^r Q_{ij}$. Moreover, it is worth mentioning that the computed values for ${}_S E_3^*$ and ${}_S \nu_{32}^*$ in Fig. 19.3 are comparable with those obtained experimentally in Hassanpour and Heppler (2017). Indeed, the experimental values for the torsional micropolar Young's modulus and twist Poisson's ratio are, respectively, equal to 0 and -1. The slight difference, highlighted in the present plots, is likely due to the presence of the interface and numerical approximations.

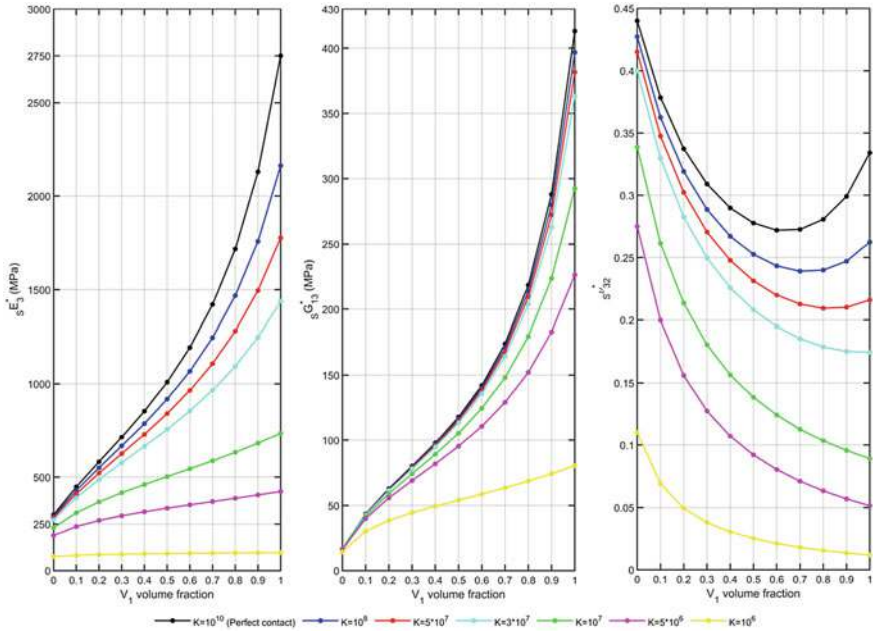

Fig. 19.2 Effective engineering moduli $\left({}_SE_3^*,\ {}_SG_{13}^*,\ \text{and}\ {}_S\nu_{32}^*\right)$ related to stiffness versus V_1 volume fraction of a bi-laminated Cosserat composite with uniform imperfect contact conditions

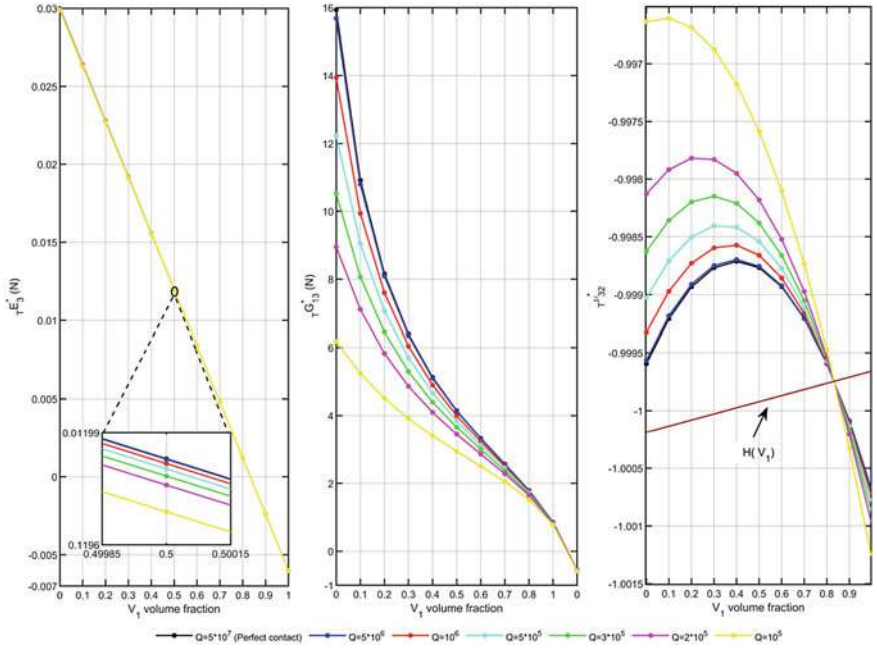

Fig. 19.3 Effective engineering moduli $\left({}_TE_3^*, {}_TG_{13}^*, \text{and}\ {}_T\nu_{32}^*\right)$ related to torque versus V_1 volume fraction of a bi-laminated Cosserat composite with uniform imperfect contact conditions

5 Conclusions

In this work, the asymptotic homogenization method is applied to heterogeneous micropolar media. In particular, effective engineering expressions with isotropic symmetry layers are provided for multi-laminated Cosserat media under non-uniform imperfect contact conditions. The effective engineering properties for centrosymmetric laminated Cosserat composites are derived as a function of the material properties, the imperfection parameters, the cell length in the y_3 direction, and the constituent's volume fractions. The typical length scales of the periodic cell and the microstructure imperfection play an important role in the macroscopic behavior of the laminate structures. The homogenized Cosserat engineering constants are characterized by two effective Young's moduli, three effective shear moduli, two effective Poisson's ratios, and two effective shear-strain ratios. Actually, only the transverse properties perpendicular to the layer distribution, i.e. along the x_3, depend on the imperfection parameter. Finally, numerical results are discussed. In general, we conclude that

(i) The stiffness $\left({}_{S}E_3^*,\ {}_{S}G_{13}^*,\ {}_{S}\nu_{31}^*\right)$ and torque $\left({}_{T}E_3^*,\ {}_{T}G_{13}^*,\ {}_{T}\nu_{31}^*\right)$ effective engineering constants transverse to the distribution of the laminae are sensible to the imperfection effects;

(ii) The effective engineering constants related to stiffness and torque, i.e. Young's moduli $E_1^* = E_2^*$, shear moduli $G_{12}^* = G_{21}^*, G_{32}^* = G_{31}^*$, Poisson's coefficient ν_{21}^*, and shear-strain ratios ζ_{2112}^* and ζ_{3223}^* are independent of the imperfection parameters and the cell length;

(iii) The volume fraction has an influence on the behavior of the stiffness and torque effective engineering moduli when the imperfect contact is considered; and

(iv) The cell length changes the effective engineering constants when imperfect contact conditions are assumed.

Acknowledgements YEA gratefully acknowledges the CONACYT for the postdoctoral scholarship "Estancias Postdoctorales por México para la Formación y Consolidación de Investigadores por México" at IIT, UACJ, 2022-2024, and the financial support of Grant A1-S-37066 during the postdoctoral stay at IIT, UACJ, 2021-2022. CFSV is grateful for the support of the CONACYT Basic Science Grant A1-S-37066. VY is grateful for the support and funding of the XS-Meta project during the course of his PhD. FJS and RRR acknowledge the funding of PAPIIT-DGAPA-UNAM IN101822, 2022-2023. This work was partially written during the visit of RRR at Aix-Marseille University, Centrale Marseille, the LMA-CNRS, and the University of Ferrara 2022. RRR thanks co-funding of the Departmental Strategic Plan, Department of Engineering, University of Ferrara. RRR would also like to thank to EDITAL UFF PROPPI No. 05/2022 and PPG-MCCT of Universidade Federal Fluminense, Brazil. This work is devoted to Igor Sevostianov, who gave significant contributions in the micro-mechanic area.

Appendix

The corresponding full approximation values with more significant digits of the effective engineering moduli ${}_S E_3^*$, ${}_S G_{13}^*$, ${}_T E_3^*$, and ${}_T G_{13}^*$ labeled with the symbol "*" in Table 19.5 are given.

Table 19.5 The values with more significant digits of the effective engineering moduli. The moduli ${}_S E_3^*$ and ${}_S G_{13}^*$ are measured in [MPa]; ${}_T E_3^*$, and ${}_T G_{13}^*$ in [N]

Moduli	V_1	$N=2$		$N=4$
		S_1	S_2	S_1
${}_S E_3^*$	0.2	0.00549993	–	–
	0.4	0.00549995	–	–
	0.6	0.00549996	–	–
	0.8	0.00549997	–	–
${}_S G_{13}^*$	0.2	0.00549937	–	–
	0.4	0.00549957	–	–
	0.6	0.00549970	–	–
	0.8	0.00549981	–	–
${}_T E_3^*$	0.2	5.48674×10^{-5}	–	–
	0.4	5.48063×10^{-5}	–	–
	0.6	5.46415×10^{-5}	–	–
	0.8	5.25861×10^{-5}	–	–
${}_T G_{13}^*$	0.2	5.49995×10^{-5}	0.00549501	0.00277542
	0.4	5.49992×10^{-5}	0.00549196	0.00277411
	0.6	5.49988×10^{-5}	0.00548791	0.00277255
	0.8	5.49979×10^{-5}	.00547929	0.00276982

References

Achenbach JD, Zhu H (1989) Effect of interfacial zone on mechanical behavior and failure of fiber-reinforced composites. J Mech Phys Solids 37(3):381–393

Adhikary DP, Dyskin DV (1997) A Cosserat continuum model for layered materials. Comput Geotech 20(1):1545

Bakhvalov N, Panasenko G (1989) Homogenization: averaging process in periodic media. In: Hills L (ed) In mathematics and its applications (Soviet Series), 1st edn. Moscow

Bigoni D, Drugan W (2007) Analytical derivation of Cosserat moduli via homogenization of heterogeneous elastic materials. J Appl Mech 74(4):741–753

Bövik P (1994) On the modelling of thin interface layers in elastic and acoustic scattering problems. Q J Mech Appl Math 47(1):17–42

Brito-Santana H, Christoff BG, Mendes Ferreira AJ, Lebon F, Rodríguez-Ramos R, Tita V (2019) Delamination influence on elastic properties of laminated composites. Acta Mech 230:821–837

Ciarlet PG (1997) Mathematical elasticity, Theory of Plates, North-Holland, Amsterdam, II

Cowin SC (1970) An incorrect inequality in micropolar elasticity theory. J Appl Math Phys 21:494–497

Dong H, Wang J, Rubin M (2014) Cosserat interphase models for elasticity with application to the interphase bonding a spherical inclusion to an infinite matrix. Int J Solids Struct 51(2):462–477

Dong H, Wang J, Rubin M (2015) A nonlinear cosserat interphase model for residual stresses in an inclusion and the interphase that bonds it to an infinite matrix. Int J Solids Struct 62:186–206

Dunn M, Ledbetter H (1995) Poisson's ratio of porous and microcracked solids: theory and application to oxide superconductors. J Mater Res 10(11):2715–2722

Duong VA, Diaz Diaz A, Chataigner S, Caronn J-F (2011) A layerwise finite element for multilayers with imperfect interfaces. Compos Struct 93:3262–3271

Ensan MN, Shahrour I (2003) A macroscopic constitutive law for elasto-plastic multilayered materials with imperfect interfaces: application to reinforced soils. Comput Geotech 30:339–345

Eringen AC (1968) Theory of micropolar elasticity. In: Liebowitz H (ed) Fracture. Academic Press, New York, pp 621–729

Eringen AC (1999) Microcontinuum field theories I: Foundations and solids. Springer, New York

Espinosa-Almeyda Y, Yanes V, Rodríguez-Ramos R, Sabina FJ, Lebon, F., Sánchez-Valdés CF, Camacho-Montes H (2022) Chapter 6: overall properties for elastic micropolar heterogeneous laminated composites with centro-symmetric constituents. In: Altenbach H, Prikazchikov D, Nobili A (eds) Book series advanced structured materials 8611, Mechanics of high-contrast elastic solids: contributions from euromech colloquium 626. Springer

Fatemi J, Van Keulen F, Onck PR (2002) Generalized continuum theories: application to stress analysis in bone. Meccanica 37:385–396

Fatemi J, Onck PR, Poort G, Van Keulen F (2003) Cosserat moduli of anisotropic cancellous bone: a micromechanical analysis. J Phys IV France 105:273–280

Forest S, Sab K (1998) Cosserat overall modeling of heterogeneous media. Mech Res Commun 25(4):449–454

Forest S, Trinh D (2011) Generalized continua and non-homogeneous boundary conditions in homogenisation methods. J Appl Math Mech ZAMM 91(2):90–109

Forest S, Padel F, Sab K (2001) Asymptotic analysis of heterogeneous Cosserat media. Int J Solids Struct 38:4585–4608

Geymonat G, Hendili S, Krasucki F, Serpilli M, Vidrascu M (2014) Asymptotic expansions and domain decomposition. In: Erhel J, Gander M, Halpern L, Pichot G, Sassi T, Widlund O (eds) Domain decomposition methods in science and engineering XXI. Lecture notes in computational science and engineering, vol 98. Springer, Cham

Goda I, Assidi M, Belouettar S, Ganghoffer JF (1990) Fracture mechanics of bone with short cracks. J Biomech 23:967–975

Gorbachev VI, Emel'yanov AN (2014) Homogenization of the Equations of the Cosserat Theory of Elasticity of Inhomogeneous Bodies. Mech Solids 49(1):73–82

Gorbachev V, Emel'yanov A (2021) Homogenization of problems of Cosserat theory of elasticity of composites. Additional materials. In: International scientific symposium in problems of mechanics of deformable solids dedicated to A.A. I1'Yushin on the occasion of his 100th birthday 49:81–88, [in Russian]

Hashin Z (2002) Thin interphase/imperfect interface in elasticity with application to coated fiber composites. J Mech Phys Solids 50(12):2509–2537

Hassanpour S, Heppler GR (2017) Micropolar elasticity theory: a survey of linear isotropic equations, representative notations, and experimental investigations. Math Mech Solids 22:224–242

Hussan JR, Trew ML, Hunter PJ (2012) A mean-field model of ventricular muscle tissue. J Biomech Eng 134(7):071003

Jasiuk I (2018) Micromechanics of bone modeled as a composite material. In: Meguid S, Weng G (eds) Micromechanics and nanomechanics of composite solids. Springer, Cham

Khoroshun LP (2019) Effective elastic properties of laminated composite materials with interfacial defects. Int Appl Mech 55:187–198

Kumari R, Singh AK, Chaki MS (2022) Influence of abrupt thickening on the shear wave propagation on reduced cosserat media with imperfect interface. Int J Geomech 22(4):04022018
Lakes R (1993) Materials with structural hierarchy. Nature 361:511–515
Lakes R, Nakamura S, Behiri J, Bonfield W (1990) Fracture mechanics of bone with short cracks. J Biomech 23:967–975
Lebée A, Sab K (2010) A Cosserat multiparticle model for periodically layered materials. Mech Res Commun 37:293–297
Nika G, On a hierarchy of effective models for the biomechanics of human compact bone tissue. HAL Id: hal-03629864
Park HC, Lakes RS (1987) Fracture mechanics of bone with short cracks. J Biomech 23:967–975
Pobedrya B (1984) Mechanics of composite materials, 1st edn. Izd-vo MGU, Moscow (in Russian)
Riahi A, Curran JH (2009) Full 3D finite element Cosserat formulation with application in layered structures. Appl Math Model 33:3450–3464
Riahi A, Curran JH (2009) Full 3d finite element Cosserat formulation with application in layered structures. Appl Math Modell 33:3450–3464
Riahi A, Curran JH (2010) Comparison of the Cosserat continuum approach with finite element interface models in a simulation of layered materials. Trans A: Civ Eng 17(1):39–52
Rodríguez-Ramos R, Yanes V, Espinosa-Almeyda Y, Otero JA, Sabina FJ, Sánchez-Valdés CF, Lebon F (2022) Micro-macro asymptotic approach applied to heterogeneous elastic micropolar media. Analysis of some examples. Int J Solids Struct 111444:239–240
Rubin MB, Benveniste Y (2004) A Cosserat shell model for interphases in elastic media. J Mech Phys Solids 52(5):1023–1052
Sack KL, Skatulla S, Sansour C (2016) Biological tissue mechanics with fibres modelled as one-dimensional Cosserat continua. Applications to cardiac tissue. Int J Solids Struct 81:84–94
Sanchez-Palencia E (1980) Non-homogeneous media and vibration theory. Springer, Berlin, Heidelberg
Serpilli M (2018) On modeling interfaces in linear micropolar composites. Math Mech Solids 23(4):667–685
Serpilli M (2019) Classical and higher order interface conditions in poroelasticity. Ann Solid Struct Mech 11:1–10
Serpilli M, Krasucki F, Geymonat G (2013) An asymptotic strain gradient Reissner–Mindlin plate model. Meccanica 48(8):2007–2018
Serpilli M, Rizzoni R, Rodríguez-Ramos R, Lebon F, Dumont S (2022) A novel form of imperfect contact laws in flexoelectricity. Comp Struct 300:116059
Sertse H, Yu W (2017) Three-dimensional effective properties of layered composites with imperfect interfaces. Adv Aircr Spacecr Sci 4(6):639–650
Tanaka M, Adachi T (1999) Lattice continuum model for bone remodeling considering microstructural optimality of trabecular architecture. In: Pedersen P, Bendsoe MP (eds) Proceedings of the IUTAM symposium on synthesis in bio solid mechanics. Kluwer Academic Publishers, The Netherlands, pp 43–54
Videla J, Atroshchenko E (2017) Analytical study of a circular inhomogeneity with homogeneously imperfect interface in plane micropolar elasticity. Z Angew Math Mech 97(3):322–339
Yanes V, Sabina FJ, Espinosa-Almeyda Y, Otero JA, Rodríguez-Ramos R (2022) Asymptotic homogenization approach applied to Cosserat heterogeneous media. In: Andrianov I, Gluzman S, Mityushev V (2022) Mechanics and physics of structured media. Academic Press, Elsevier, USA
Yang JFC, Lakes RS (1981) Transient study of couple stress in compact bone: torsion. J Biomech Eng 103:275–279
Yang JFC, Lakes RS (1982) Experimental study of micropolar and couple-stress elasticity in bone in bending. J Biomech 15:91–98